Dynamic Decoherence Control of a Solid-State Nuclear-Quadrupole Qubit

E. Fraval,* M. J. Sellars, and J. J. Longdell

Laser Physics Centre, Research School of Physical Sciences and Engineering, Australian National University, Canberra, ACT, 0200, Australia

(Received 5 January 2005; published 15 July 2005)

We report on the application of a dynamic decoherence control pulse sequence on a nuclear-quadrupole transition in Pr^{3+}:Y_2SiO_5. Process tomography is used to analyze the effect of the pulse sequence. The pulse sequence was found to increase the decoherence time of the transition to over 30 seconds. Although the decoherence time was significantly increased, the population terms were found to rapidly decay on the application of the pulse sequence. The increase of this decay rate is attributed to inhomogeneity in the ensemble. Methods to circumvent this limit are discussed.

DOI: 10.1103/PhysRevLett.95.030506 PACS numbers: 03.67.Pp, 76.30.Kg, 76.60.−k, 76.70.Hb

Recent experiments have demonstrated that optically active centers in solids and, in particular, rare-earth ions in crystals, show promise as an alternative to atomic based ensembles for quantum information processing applications [1,2]. Rare-earth doped ions provide multilevel systems possessing optical transitions with long coherence times, and in crystalline hosts high optical densities are achievable.

A common feature of many of the proposed ensemble based quantum information processing applications—including quantum memories, single photon sources, and quantum repeaters—involves the storage of quantum information on long lived low lying states [3–5]. Solid-state centers have the significant advantage over atomic systems that they are stationary and hence the duration which quantum information can be stored is limited by the decoherence time of the states and not by the motion of the ensemble. In the case of rare-earth centers it is proposed to store the quantum information on the centers' ground state hyperfine transitions [6,7]. The decoherence times of hyperfine transitions in rare-earth centers are typically of the order of ms but in recent work we have demonstrated a method to extend the decoherence time to 82 ms in the case of $m_I = -1/2 \leftrightarrow +3/2$ transition in Pr^{3+}:Y_2SiO_5 [8]. In this Letter we demonstrate a further dramatic increase of the coherence time to several tens of seconds through the use of a dynamic decoupling sequence.

Dynamic decoupling methods for open systems were initially developed for use in NMR spectroscopy to selectively remove contributions to the spin Hamiltonian [9,10]. There is growing interest in applying these decoupling techniques to quantum information systems to decrease their rate of decoherence [11–15]. Sequences of interest decouple the quantum system from the surrounding thermal bath through the application of a periodic control Hamiltonian. In the current work this is implemented by a series of π pulses with alternating 0° and 180° phase shifts separated by the cycling time τ_c. The alternating phase shift minimizes the accumulation of errors due to pulse imperfections [16]. The decoupling pulse sequence can theoretically rephase all the coherence in the quantum system, thereby making $T_2 = T_1$ if the following criteria [11] are met:

$$\omega_c \tau_c \lesssim 1, \tag{1}$$

where ω_c is the cutoff frequency of the dephasing bath and the pulses are "hard," such that during the pulse any evolution of the state other than the action of the driving field can be assumed to be negligible.

For Pr ions substituting for Y in Y_2SiO_5 the main source of decoherence of the ground state hyperfine transitions is magnetic interactions with nuclei in the host [8,17]. ^{89}Y possess a nuclear spin of 1/2 with a gyromagnetic ratio of 209 Hz/G. The other nuclear spin in the host is ^{29}Si found in natural abundance (~ 4%) with a moment of 845 Hz/G. The magnetic field seen by any given Pr ion fluctuates over time due to resonant cross relaxations between the host spins. The sensitivity can be calculated using the reduced Hamiltonian of the electronic ground state hyperfine structure [1]. Praseodymium has a nuclear spin of 5/2, and as a result of a pseudoquadrupole interaction its electronic ground state splits into three doubly degenerate levels with splittings of the order of 10 MHz. The final degeneracy can be lifted by a magnetic field through an enhanced nuclear Zeeman interaction.

In the region where the applied field produces anticrossings, a field direction and magnitude can be found such that there is no first order Zeeman shift for a field perturbation in any direction for the $m_I = -1/2 \leftrightarrow +3/2$ hyperfine transition, as demonstrated in recent work [8]. This magnetic field alignment will be referred to as the *critical point* to reflect the zero gradient in the Zeeman splitting. It has been shown that the dephasing perturbations acting on the Pr ions are predominantly occurring on a time scale longer than ~10 ms [8]. Given that Rabi frequencies greater than 100 kHz are readily achievable, the period between the applied pulses in the decoupling sequence can be made such that the inequality (1) is satisfied for the frequencies of the dominant perturbations.

 © 2005 The American Physical Society

As in previous work a Pr^{3+}:Y_2SiO_5 0.05% concentration crystal is maintained at temperature of ~1.5 K in a liquid helium bath cryostat [8]. Yttrium orthosilicate (Y_2SiO_5) is a low symmetry host with two crystallographically inequivalent sites where Pr can substitute for Y in two sites, labeled ''site 1'' and ''site 2'' [18]. Site 1 ions are used in this work. In the coordinate system chosen to describe the magnetic field the C_2 axis is y, z is the direction of the predominate polarization of the optical $^3H_4$-$^1D_2$ transition, and x is perpendicular to both.

The magnetic fields to achieve the critical point field configuration $\boldsymbol{B}_{CP} = 732, 173, -219$ G [8] are supplied by two orthogonal superconducting magnets aligned with the z axis and in the x, y plane. The sample was rotated about the z axis to provide the correct ratio of fields along the x and y axes for the critical point in magnetic field space. The field in the x, y plane could also be adjusted using a small correction coil mounted orthogonal to the main coil. The inhomogeneity in magnetic field across the sample was measured using a hall probe to be <2 G.

Raman heterodyne was employed to investigate the ground state hyperfine transitions using an experimental configuration similar to that described in previous work [8]. The experiment was performed using a Coherent 699 frequency stabilized tunable dye laser tuned to the $^3H_4$-$^1D_2$ transition at 605.977 nm. The commercial laser's frequency was further stabilized to a subkilohertz linewidth. The laser power incident on the crystal was 40 mW, focused to ~100 μm and could be gated using a 100 MHz acousto-optic modulator. The hyperfine transition was excited using a six turn coil with a diameter of 5 mm, driven by a 10 W radio frequency (RF) amplifier resulting in a Rabi frequency $\Omega_{RF} = 91$ kHz. The RF pulse and digital control sequences were generated using a direct digital synthesis system referenced to an oven controlled crystal oscillator. The pulse sequences used in the experiment are illustrated in Fig. 1(a). The Raman heterodyne signal, seen as a beat on the optical beam, was detected by a 125 MHz photodiode. This signal was analyzed using a mixer and a phase controlled local oscillator referenced to the RF driving field.

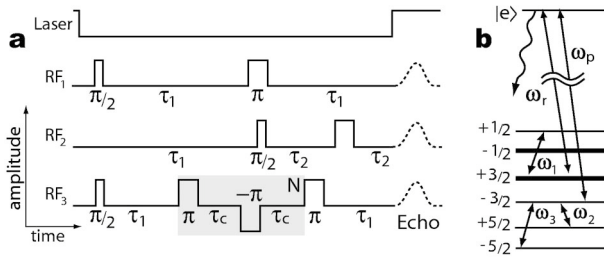

FIG. 1. (a) Pulse sequences used in experiment: RF_1: 2 pulse spin echo, RF_2: Inversion Recovery RF_3: Decoupling pulse sequence. The coherence generated by the initial pulse is rephased by a pair of π, $-\pi$ pulses separated by the cycling time τ_c, iterated N times. The laser is common to all pulse sequences. (b) All ground state hyperfine levels other than $m_I = -1/2$ interact via RF frequencies ω_1, ω_2, ω_3 with laser radiation either at the read frequency ω_r or pump frequency ω_p. Through spontaneous emission from the electronic excited state the group of ions interacting with both ω_r and ω_p via any common excited state will be optically pumped into the $m_I = -1/2$ state. Bold states are the critical point transition.

At the critical point field the $m_I = -1/2 \leftrightarrow +3/2$ transition was observed at 8.646 MHz with a inhomogeneous linewidth of 4 kHz. This linewidth was found to be insensitive to changes in the magnetic field of the order of ~10 G.

Prior to applying each Raman heterodyne pulse sequence the sample was prepared with the optical/RF repump scheme as shown in Fig. 1(b). The repump frequencies were $\omega_r - \omega_p = 18.2$ MHz, $\omega_1 = 12.2$ MHz, $\omega_2 = 15.35$ MHz, and $\omega_3 = 16.3$ MHz. The repump RF was pulsed with a duty cycle of 10% to reduced sample heating, while the repump laser frequency ω_r was scanned 200 kHz to hole burn a ''trench'' in the inhomogeneous optical line centered at ω_r. This repump scheme ensures that all Pr ions interacting with the laser radiation are forced into the $m_I = -1/2$ state, creating a pure state ensemble. It also ensures there is no initial population at the laser frequency used for Raman heterodyne detection. The use of a subkilohertz linewidth laser and the repump scheme resulted in a significant improvement in the signal to noise compared to work performed earlier [8].

To determine T_2 at and near the critical point we measured the amplitude of two pulse spin echoes as a function of the delay between the pulses, as shown in Fig. 2. Three data sets are shown. The first is for the critical point magnetic field alignment, optimized by maximizing the echo amplitude at long decay times, while the others are for the field detuned by 2 and 5 G in the z direction from this optimal value. The significantly longer decay time compared to previous work [8] is attributed to better identification of the critical point using more precise magnetic

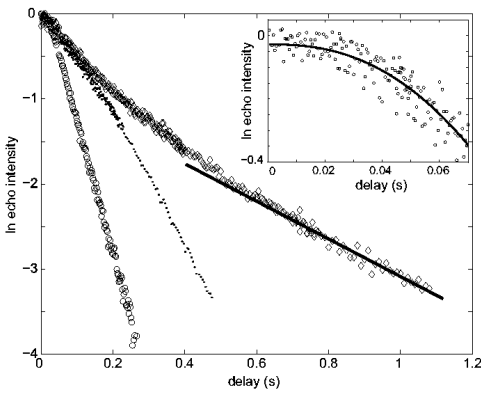

FIG. 2. Spin echo decay at the critical point field (◇) and detuned from the critical point field by ~2 G (·) and ~5 G (○) in the Z direction).

field adjustments. Besides being longer, the decay can no longer be described by standard echo decay function with a single time constant [19]. There are three distinct regions. For pulse separations less than 20 ms, the decay rate is less than $1/4$ s^{-1}. At 30 ms there is a distinct shoulder with the decay rate increasing to $1/0.4$ s^{-1} as the pulse separation reaches 60 ms. From 150 ms onwards the decay rate asymptotically approaches a value of $1/0.86$ s^{-1}. This asymptotic decrease in the decay rate was only observed for magnetic fields within 0.5 G of the optimal field. When the field was more than 0.5 G away from the critical point a simple exponential decay was observed for delays longer than 50 ms.

The shoulder in the decay at 30 ms is interpreted as indicating that the majority of the dephasing is due to perturbations that occur on time scales between 10 and 100 ms. The asymptotic behavior of the decay is attributed to a variation in the T_2 within the ensemble resulting from inhomogeneity in the magnetic field across the sample. Ions experiencing a field closer to the critical point condition will have a longer T_2 and consequently their contribution to the echo intensity will dominate for long pulse separations. The asymptotic decay rate therefore gives an upper limit for the contribution to the decoherence rate due to second order magnetic interactions.

The decoupling pulse sequence was investigated using an initial delay of $\tau_1 = 1.2$ ms and varying the cycling time τ_c from 20 ms to 0.5 ms, as shown in Fig. 3. Also shown in Fig. 3 is the result of an inversion recovery measurement used to determine the lifetime of the transition. The inversion recovery measurements were performed using the pulse sequence described in Fig. 1(a). As can be seen in Fig. 3 the decoupling sequence significantly increases T_2, though T_2/T_1 is less than $1/4$, even for the shortest value of τ_c. In Fig. 4 the coherence times T_2 for each of the data sets are plotted as a function of the cycling time τ_c. This shows that for $\tau_c < 5$ ms, as τ_c is reduced T_2 significantly increases, while further reducing τ_c, T_2 only increases slightly. The measurements were repeated with the dc magnetic field detuned by 5 G, also shown in Fig. 4.

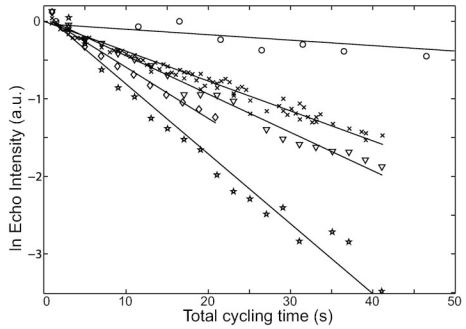

FIG. 3. Decoupled echo decays with $\tau_c = 7.5$ ms (\star), 10 ms ($\diamond$), 15 ms (∇), 20 ms ($\times$) corresponding to $T_2 = 27.9$, 21.1, 15.2, 10.9 s. Inversion recovery measurements ($\bigcirc$) yield $T_1 = 145$ s.

The field detuning increases the transition's magnetic field sensitivity, such that the two pulse echo T_2 was reduced to $\sim$100 ms. For $\tau_c < 5$ ms, T_2 is lower but has a similar dependence on τ_c. As τ_c is decreased further, T_2 asymptotically approaches the same limit observed for the optimized critical point. This observation suggests that the residual decoherence in the limit of short τ_c is not due to magnetic field fluctuations. The residual decoherence may be due to detuning and pulse area errors in the decoupling sequence.

To assess the action of the decoupling sequence on an arbitrary quantum state we determine the process operator, $\mathcal{O}$, by performing quantum process tomography [20]. Quantum process tomography was performed on the input state and for 1, 10, 100, and 1000 iterations of the decoupling sequence. The initial delay was $\tau_1 = 1.2$ ms, with a cycling time of $\tau_c = 2$ ms. The total period over which the tomography was performed was $\sim$4 ms, $\sim$40 ms, $\sim$400 ms, and $\sim$4 s, respectively. The imaginary component of the process operator was omitted for clarity as its magnitide was less than 10% of the real component for all cases studied. Ideally the decoupling sequence process operator is the identity matrix, as it should leave the state unchanged, while the worst case is the process operator results in an incoherent state (nonzero elements: $\mathcal{O}_{11} = \mathcal{O}_{44} = \mathcal{O}_{14} = \mathcal{O}_{41} = 0.5$). It can be seen from Fig. 5 that the population terms rapidly decay toward the incoherent state. The coherence terms ($\mathcal{O}_{22}$, $\mathcal{O}_{33}$), however, persist for significantly longer with the process operator components remaining nonzero even after 1000 decoupling cycles.

The evolution of the ensemble was modeled using the Bloch equations assuming an infinite T_1 and T_2, with an inhomogeneous linewidth of 4 kHz (FWHM) and a Rabi frequency of 100 kHz. The results from this modeling are shown in Fig. 5, alongside the experimental data. Despite the model not including any homogeneous dephasing, the rapid decay of population terms compared to coherence terms of the simulated process tomography (Fig. 5) match the experimental data. Simulations indicate that the decay rate of the population terms can be reduced by increasing the ratio of the Rabi frequency to the linewidth. A suitable criterium for when the application of the decoupling sequence is useful for preserving arbitrary quantum states is

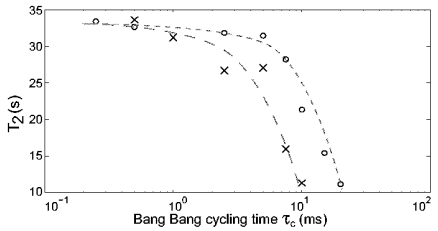

FIG. 4. Dependence of decoherence time on the decoupling sequence cycling time τ_c both at the critical point ($\bigcirc$) and with the magnetic field misaligned to give a coherence time of $T_2 =$ 100 ms ($\times$). Lines do not represent a physical model.

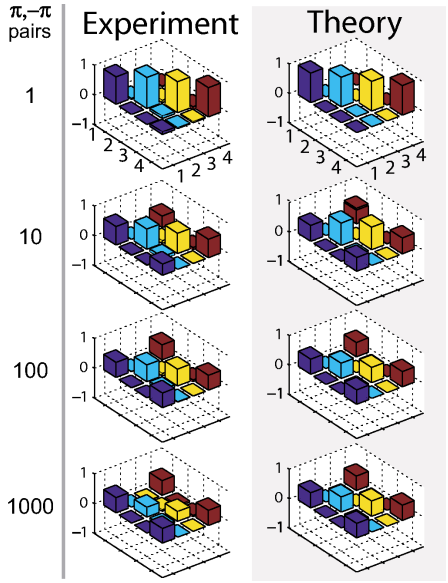

FIG. 5 (color). Comparison of experimental to theoretical process tomography results for the decoupling pulse sequence with 1, 10, 100, and 1000 iterations. Imaginary components omitted for clarity. The states are labeled 1, 2, 3, 4 corresponding to $|0\rangle\times\langle 0|$, $|0\rangle\langle 1|$, $|1\rangle\langle 0|$, and $|1\rangle\langle 1|$.

when the decay rate of the population terms in the presence of the pulse sequence is slower than that of the coherence terms in the absence of the decoupling sequence. For the present case where $T_2 = 0.86$ s the simulation indicates that to meet these criteria it will be necessary to achieve a ratio of Rabi frequency to linewidth of $\Omega_{\mathrm{RF}}/\omega_{inh} \approx 100$. There is limited capacity to increase the Rabi frequency of the driving field without the possible excitation of off-resonant transitions. Therefore, for the application of the decoupling sequence to the $m_I = -1/2 \leftrightarrow +3/2$ transition to be useful it will be necessary to reduce the inhomogeneous broadening of the transition by a factor of ~ 10.

The large change in magnetic field sensitivity as the critical point field is approached with no corresponding change in the inhomogeneous linewidth of the transition suggests that the inhomogeneous broadening of the transition at the critical point field is not due to magnetic interactions. The inhomogeneous broadening at the critical point field is probably due to strain within the crystal which is not intrinsic to the site and can be reduced by refining standard crystal growing techniques. A reduction in strain broadening by over an order of magnitude has been achieved in analogous materials [21] through reducing the dopant concentration. Irrespective of reaching the desired ratio of Rabi frequency to inhomogeneous linewidth, methods of designing pulse sequences more robust to Rabi and detuning errors have been proposed [22,23].

In conclusion, the application of the decoupling sequence demonstrates that dynamic decoupling techniques are applicable to correcting quantum errors on nuclear spin transitions of Pr^{3+}:Y_2SiO_5. This work realizes very long hyperfine decoherence times, greater than 30 s, in a solid-state optical Λ system, suitable for quantum information processing applications.

The support of this work by the Defence Science Technology Organization (DSTO) and the Australian Research Council (ARC) is gratefully acknowledged.

*Electronic address: elliot.fraval@anu.edu.au

[1] J. J. Longdell, M. J. Sellars, and N. B. Manson, Phys. Rev. B **66**, 035101 (2002).
[2] J. J. Longdell and M. J. Sellars, Phys. Rev. A **69**, 032307 (2004).
[3] B. Julsgaard, J. Sherson, J. I. Cirac, J. Fiurasek, and E. S. Polzik, Nature (London) **432**, 482 (2004).
[4] A. Kuhn, M. Hennrich, and G. Rempe, Phys. Rev. Lett. **89**, 067901 (2002).
[5] H. J. B. W. Dür, J. I. Cirac, and P. Zoller, Phys. Rev. Lett. **81**, 5932 (1998).
[6] N. Ohlsson, R. K. Mohan, and S. Kröll, Opt. Commun. **201**, 71 (2002).
[7] S. A. Moiseev and S. Kröll, Phys. Rev. Lett. **87**, 173601 (2001).
[8] E. Fraval, M. Sellars, and J. J. Longdell, Phys. Rev. Lett. **92**, 077601 (2004).
[9] P. T. Callaghan, *Principals of Nuclear Magnetic Resonance Microscopy* (Oxford University Press, New York, 1991).
[10] E. L. Hahn, Phys. Rev. **80**, 580 (1950).
[11] L. Viola and S. Lloyd, Phys. Rev. A **58**, 2733 (1998).
[12] L. Viola, E. Knill, and S. Lloyd, Phys. Rev. Lett. **82**, 2417 (1999).
[13] L. Viola, J. Mod. Opt. **51**, 2357 (2004).
[14] M. S. Byrd and D. A. Lidar, Phys. Rev. Lett. **89**, 047901 (2002).
[15] D. Vitali and P. Tombesi, Phys. Rev. A **59**, 4178 (1999).
[16] S. Meiboom and D. Gill, Rev. Sci. Instrum. **29**, 688 (1958).
[17] E. Fraval, M. J. Sellars, A. Morrison, and A. Ferris, J. Lumin. **107**, 347 (2004).
[18] R. W. Equall, R. L. Cone, and R. M. Macfarlane, Phys. Rev. B **52**, 3963 (1995).
[19] W. B. Mims, Phys. Rev. **168**, 370 (1968).
[20] M. A. Nielsen and I. L. Chuang, *Quantum Computation and Quantum Information* (Cambridge University Press, Cambridge, England, 2000), 1st ed..
[21] R. M. Macfarlane, R. S. Meltzer, and B. Z. Malkin, Phys. Rev. B **58**, 5692 (1998).
[22] L. Viola and E. Knill, Phys. Rev. Lett. **90**, 037901 (2003).
[23] P. Wocjan, quant-ph/0410107.